Verified Stability Analysis for Interval-Based Sliding Mode and Predictive Control Procedures with Applications to High-Temperature Fuel Cell Systems

Andreas Rauh * **Luise Senkel** * **Julia Kersten** *
Harald Aschemann *

* *Chair of Mechatronics, University of Rostock, D-18059 Rostock, Germany (e-mail: {Andreas.Rauh,Luise.Senkel,Julia.Kersten,Harald.Aschemann}@uni-rostock.de)*

Abstract: In previous work, control-oriented models have been derived for solid oxide high-temperature fuel cell systems. In these models, interval variables have been used to describe uncertainty due to a limited knowledge about system parameters and to handle effects of electric load variations on the temperature distribution in the fuel cell stack module as well as bounded measurement uncertainty. To deal with these types of uncertainty both in the design of robust controllers and during their online usage, interval techniques can be employed successfully. These control procedures make use of the basic principles of either sliding mode control or predictive control. The corresponding algorithms and the prerequisites for their real-time capable implementation using software libraries for interval arithmetic and algorithmic differentiation are described in this paper. Experimental results show the efficiency of these control laws for a fuel cell test rig that is available at the Chair of Mechatronics at the University of Rostock.

Keywords: Interval arithmetic, sliding mode control, predictive control, fuel cell systems

1. INTRODUCTION

Both the efficiency and life time of high-temperature fuel cells are significantly influenced by the temperature distribution in the interior of fuel cell stack modules. However, it is not possible to determine all parameters affecting the thermal fuel cell behavior with absolute accuracy. The same holds for the limited capabilities of measuring the stack temperature. Typically, this temperature is only measurable at a few selected positions in the interior of the stack module, where the measurements are subject to quite large uncertainty. For these reasons, it is essential to develop robust, guaranteed stabilizing control strategies which have to be capable of dealing with the following issues:

- The control strategies have to be applicable in wide operating ranges as well as in transient operating conditions during heating and cooling phases of the stack module; such wide operating ranges typically lead to the necessity of employing nonlinear thermal fuel cell models.
- The above-mentioned uncertainties, representable by means of bounded intervals, and external disturbances due to electrical load variations shall be taken into account during the guaranteed stabilizing control design.
- It shall be possible to change the position at which the stack temperature is controlled during system operation.
- Large spatial gradients of the stack temperature have to be counteracted by the control law to prevent accelerated degradation of the stack module.
- To maximize the overall efficiency, the system inputs shall be chosen according to a suitable optimality criterion.

Due to the requirements listed above, novel interval-based sliding mode control strategies and robust sensitivity-based control procedures are designed in this paper and analyzed with respect to their robustness and stability properties. To show their efficiency for real-life fuel cell systems, the corresponding alternative control strategies are derived for a mathematical model of a Solid Oxide Fuel Cell system (SOFC system) corresponding to a test rig at the Chair of Mechatronics, University of Rostock. First experimental results for selected control laws, implemented on this test rig, are presented.

This paper is structured as follows: In Sec. 2, an overview of the design of control-oriented mathematical models for SOFC systems is given. Sec. 3 summarizes the basic procedures for the design of interval-based sliding mode controllers of the thermal behavior of the SOFC test rig. Here, the control input is characterized by the enthalpy flow of cathode gas that is supplied to this system. In the practical implementation, this enthalpy flow has to be provided by subsidiary controllers for the corresponding mass flow and temperature of the cathode gas. In Sec. 4, a predictive control strategy — which can be used instead of the sliding mode approach — is presented which allows for a direct computation of the above-mentioned quantities. Finally, conclusions and an outlook on future work are given in Sec. 5.

2. THERMAL BEHAVIOR OF SOFC SYSTEMS

The implementation of real-time capable robust control strategies for the thermal behavior of SOFC systems makes use of low-dimensional finite volume models with a flexible spatial resolution of the stack module's temperature distribution. As shown in (Rauh et al., 2011), this thermal system model can be interconnected with further submodels characterizing the fluidic and electrochemical properties of the SOFC. However, these interconnected subsystems can be considered as disturbance inputs when focusing on the temperature control of the SOFC.

To describe the thermal behavior of an SOFC with sufficient accuracy for control purposes, integral energy balances are derived in the form of a finite volume model, given in terms of a coupled set of nonlinear ordinary differential equations (ODEs). In these ODEs, the following effects depicted in Fig. 1 are included: internal heat conduction and enthalpy flows of the anode gas (AG) and cathode gas (CG) with temperature-dependent heat capacities, exothermic reaction processes ($\dot{Q}_R$) with temperature-dependent reaction enthalpies, heat transfer between the stack module and the ambient medium ($\dot{Q}_A$) as well as heat production due to internal Ohmic losses (P_{El}), cf. (Bove and Ubertini, 2008; Rauh et al., 2011, 2012a).

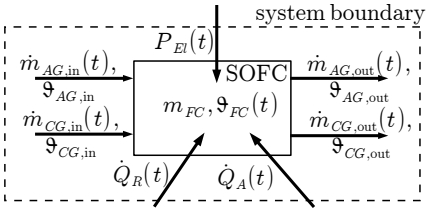

Fig. 1. Integral energy balance for the SOFC stack module.

The exothermic reaction between the fuel gas supplied at the anode (in this paper, pure hydrogen) and the cathode gas (air) results from the electrochemical reaction

$$2\,H_2 + 2O^{2-} \rightarrow 2\,H_2O + 4e^- \quad \text{and} \quad O_2 + 4e^- \rightarrow 2O^{2-} \quad (1)$$

taking place at the anodes and cathodes in the SOFC stack. To develop robust control strategies, it is essential to be able to cope with non-stationary operating points of the SOFC, in which the heat production due to the exothermic reaction (1) as well as the Ohmic losses in the interior of the stack module are time-dependent. This is caused by an a-priori unknown variation of the demand for the electrical power to be supplied to a consumer.

To reduce thermal stress in the stack module materials, which inevitably leads to an accelerated degradation of the fuel cell, it is essential to keep the system temperature as close as possible to a desired set-point. Simultaneously, spatial gradients of the internal stack temperature have to be minimized effectively despite external disturbances.

For that reason, the temperature distribution in the SOFC stack is described by a finite volume model with a flexible spatial resolution. The complexity of this model ranges from a global system model, which only provides one lumped temperature for the complete SOFC system, to finite volume models in which the temperature distribution is described after a semi-discretization into $n_x = L \cdot M \cdot N$ finite volume elements, cf. Fig. 2 and (Rauh et al., 2012a).

In Fig. 2, the variables L, M and N represent the numbers of finite volume elements along each space coordinate which can be chosen in a problem-oriented way. For each volume element (i, j, k), an integral energy balance (according to the effects described above)

$$\begin{aligned} c_{i,j,k} m_{i,j,k} \dot{\vartheta}_{i,j,k}(t) = {} & C_{AG,i,j,k}(\vartheta, t)\,[\vartheta_{i,j-1,k}(t) - \vartheta_{i,j,k}(t)] \\ & + C_{CG,i,j,k}(\vartheta, t)\,[\vartheta_{i,j-1,k}(t) - \vartheta_{i,j,k}(t)] \\ & + \dot{Q}_{\eta,i,j,k}(t) + \dot{Q}_{R,i,j,k}(t) + P_{El,i,j,k}(t) \end{aligned} \quad (2)$$

is set up with the local specific heat capacity $c_{i,j,k}$ and the local mass parameter $m_{i,j,k}$.

By including the inter-element conditions characterizing the continuity of the heat flow over each boundary surface between neighboring finite volume elements, a set of ODEs

$$\dot{\mathbf{x}}(t) = \mathbf{f}\left(\mathbf{x}(t), \mathbf{p}, \mathbf{u}(t)\right) \quad (3)$$

is obtained with the states $\mathbf{x}^T = [\vartheta_{1,1,1} \ \ldots \ \vartheta_{L,M,N}] \in \mathbb{R}^{n_x}$. The parameters $\mathbf{p}$ can be identified experimentally as described in (Rauh et al., 2012a,c). Moreover, the control vector $\mathbf{u}$ consists of the mass flow $\dot{m}_{CG,in}$ of preheated cathode gas with the temperature $\vartheta_{CG,in}$.

In (2), the term

$$\dot{Q}_{\eta,i,j,k}(t) = \sum_{\eta \in \mathcal{N}} \frac{1}{R_{th,\eta}^{i,j,k}} \left(\vartheta_\eta(t) - \vartheta_{i,j,k}(t)\right) \quad (4)$$

characterizes the heat transfer and the heat conduction by the thermal resistance $R_{th,\eta}^{i,j,k}$ from all neighboring volume elements denoted by the multi index $\eta \in \mathcal{N}$ to the volume element i, j, k. In (4), the resistances for heat conduction in the interior of the semi-discretized fuel cell stack module are distinguished from thermal resistances for finite volume elements with a direct connection to the environment, leading to different values for the corresponding variables $R_{th,\eta}^{i,j,k}$ in the parameter identification. Here, the thermal resistances on the system boundary are typically larger due to the insulation layer than the ones in the interior of the fuel cell stack module which correspond to an averaged material parameter of the electrodes, the solid electrolytes, and the interconnection layers. The term $(\vartheta_\eta - \vartheta_{i,j,k})$ represents either the temperature difference between neighboring finite volume elements in the interior of the stack or the temperature difference to the surrounding air. Here, the temperatures of the neighboring elements are denoted by ϑ_η, while ϑ_A is the ambient temperature.

The reaction enthalpy is included in (2) by

$$\dot{Q}_{R,i,j,k}(t) = \frac{\Delta_R H_{i,j,k}(\vartheta_{i,j,k}) \cdot \dot{m}_{H_2,i,j,k}^R(t)}{M_{H_2}} \ , \quad (5)$$

with the local temperature-dependent molar reaction enthalpy $\Delta_R H_{i,j,k}(\vartheta_{i,j,k})$ and the local molar flow of hydrogen $\frac{\dot{m}_{H_2,i,j,k}^R}{M_{H_2}}$. Furthermore, Faraday's law yields

$$\dot{Q}_{R,i,j,k}(t) = \Delta_R H_{i,j,k}(\vartheta_{i,j,k}) \frac{I_{i,j,k}(t)}{z\ F} \quad (6)$$

with the electric current $I_{i,j,k}$ in the corresponding volume element, the Faraday constant F and the number of electrons z transferred in the overall reaction (1) (Bove and Ubertini, 2008). The electric current $I_{i,j,k}$ significantly influences the local Ohmic losses $P_{El,i,j,k}(t) = R_{El,i,j,k} I_{i,j,k}^2(t)$ with the internal resistance $R_{El,i,j,k}$. For

the computation of the heat capacities $C_{AG,i,j,k}(\vartheta_{i,j,k}, t)$ and $C_{CG,i,j,k}(\vartheta_{i,j,k}, t)$ of the fluids inside each finite volume element, the local consumption of hydrogen H_2 at the anode, of oxygen O_2 at the cathode and the local production of water vapor H_2O at the anode have to be taken into account as described in (Rauh et al., 2012a).

The temperature $\vartheta_{i,j-1,k}(t)$ of the enthalpy flows is set to ϑ_P for $j = 1$ and to ϑ_η for $1 < j \leq M$, where ϑ_P is the temperature of the preheated supply gases. This assumption serves as a simplification of the internal heat transfer process. It is justified by the large time needed for changing the internal energy of the solid material in contrast to the significantly smaller time for changing the internal energy of the supply gases. This fact results from the significant difference of the values for the corresponding heat capacities. Moreover, the following boundary conditions hold: $\vartheta_{i-1,j,k} = \vartheta_A$ for $i = 1$, $\vartheta_{i+1,j,k} = \vartheta_A$ for $i = L$, $\vartheta_{i,j-1,k} = \vartheta_P$ for $j = 1$, $\vartheta_{i,j+1,k} = \vartheta_A$ for $j = M$, and $\vartheta_{i,j,k-1} = \vartheta_A$ for $k = 1$, $\vartheta_{i,j,k+1} = \vartheta_A$ for $k = N$.

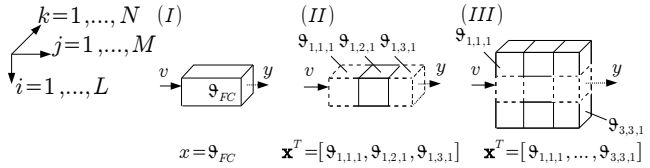

Fig. 2. Different variants of the semi-discretization of the fuel cell stack module.

In the following, control strategies are presented for the configurations (I) and (II) with possible extensions outlined for the case (III) in Fig. 2. In the case (I), the state equation (3) is characterized by a scalar state variable ($n_x = 1$), whereas the configurations (II) and (III) have $n_x = M = 3$ and $n_x = L \cdot M = 9$ state variables, respectively. Moreover, the configurations (II) and (III) contain at least one further internal state allowing for a description of spatial variations of the fuel cell temperature in the interior of the stack module. The measured system output corresponds to the temperature at the exhaust gas manifolds which is assumed to be identical to ϑ_{FC} in the case (I). In the cases (II) and (III), this temperature corresponds to $\vartheta_{1,3,1}$ and $\vartheta_{2,3,1}$, respectively. Taking further into account the measured temperature at the inlet gas manifold in the output vectors $\mathbf{y}$, it becomes possible to design both offline parameter identification procedures as well as real-time state and parameter estimators. Details about these procedures can be found in (Dötschel et al., 2013a; Rauh et al., 2012c).

If the state vectors $\mathbf{x}$ given in Fig. 2 are not fully measurable, they have to be reconstructed by a suitable observer, cf. (Rauh et al., 2012c). To account for non-negligible measurement as well as state reconstruction errors, the corresponding values are assumed to be disturbed by values for which worst-case interval bounds are known.

3. INTERVAL-BASED SLIDING MODE CONTROL

3.1 State-Space Transformation for Control Design

To design robust, interval-based sliding mode control procedures, the cases (I) and (II) according to Fig. 2 are first discussed. Second, necessary extensions are described if the control law is to be generalized to the case (III) or to the most general case of a spatial semi-discretization in all three coordinates.

In general, this design procedure is based on an input-affine system model. For the case (I), this representation can be obtained in a straightforward way as

$$\dot{\vartheta}_{FC}(t) = a\big(\vartheta_{FC}(t)\big) + b\big(\vartheta_{FC}(t)\big) \cdot v(t) \ , \quad \vartheta_{FC} \in \mathbb{R} \ , \quad (7)$$

with the state ϑ_{FC} introduced in Sec. 2, if the enthalpy flow of the cathode gas is used as the control input $v(t) = \dot{m}_{CG}(t) \cdot \big(\vartheta_{CG}(t) - \vartheta_{FC}(t)\big)$, $\vartheta_{FC}(t) = \vartheta_{1,1,1}(t)$.

In the more general case of a spatial semi-discretization along the direction of the gas mass flow, cf. the case (II), the system model has to be transformed into its nonlinear controller normal form according to the following procedure. Here, the output equation $y = h(\mathbf{x}) = \vartheta_{1,M,1}$ is differentiated with respect to time up to the derivative that depends on v explicitly. It can be shown that this degree corresponds to the number of volume elements M if the gas mass flows in the interior of the fuel cell module are assumed to be independent of v. This assumption can be made with good accuracy for sufficiently slow variations of $\dot{m}_{CG}$ as well as for high-temperature operating points, where variations of $\dot{m}_{CG}$ are prohibited by an underlying safety system for the SOFC stack. The approximation error resulting from this assumption can be accounted for by the disturbance variables described in the following.

In the case (II), successive differentiations of the output equation $y = h(\mathbf{x})$ yield the Lie derivatives

$$y^{(i)} = L_{\mathbf{f}}^i h(\mathbf{x}) = L_{\mathbf{f}} \left(L_{\mathbf{f}}^{i-1} h(\mathbf{x}) \right) , \quad i = 0, ..., \delta - 1 \qquad (8)$$

with $y = h(\mathbf{x}) = L_{\mathbf{f}}^0 h(\mathbf{x})$ for $i = 0$ and the relative degree $\delta = M$, see (Marquez, 2003).

Assuming that the direct influence of $v(t)$ on the state variables $\vartheta_{1,2,1}, \ldots, \vartheta_{1,M,1}$ due to variations of $\dot{m}_{CG}$ is sufficiently small, the relation $\frac{\partial L_{\mathbf{f}}^i h(\mathbf{x})}{\partial v} = 0$ holds for all $i = 0, \ldots, M-1$. Using the new state vector

$$\mathbf{z}^T = \left[h(\mathbf{x}) \ L_{\mathbf{f}} h(\mathbf{x}) \ \ldots \ L_{\mathbf{f}}^{M-1} h(\mathbf{x}) \right]^T \in \mathbb{R}^M \ , \qquad (9)$$

the state equations (3) of the case (II) can be transformed into the nonlinear state-space representation

$$\dot{\mathbf{z}} = \begin{bmatrix} L_{\mathbf{f}} h(\mathbf{x}) \\ \vdots \\ L_{\mathbf{f}}^{M-1} h(\mathbf{x}) \\ L_{\mathbf{f}}^{M} h(\mathbf{x}) \end{bmatrix} = \begin{bmatrix} z_2 \\ \vdots \\ z_M \\ \tilde{a}(\mathbf{z}, \mathbf{p}, d) \end{bmatrix} + \begin{bmatrix} 0 \\ \vdots \\ 0 \\ \tilde{b}(\mathbf{z}, \mathbf{p}) \end{bmatrix} \cdot v \qquad (10)$$

with an additive bounded disturbance $d \in [d] = \left[\underline{d} \, ; \, \overline{d}\right]$ and the interval parameters $\mathbf{p} \in [\mathbf{p}]$ with $\mathbf{p} \in \mathbb{R}^{n_p}$. Hence, the term $\tilde{a}$ is defined as $\tilde{a}(\mathbf{z}, \mathbf{p}, d) = L_{\mathbf{f}}^M h(\mathbf{x}) - \tilde{b}(\mathbf{z}, \mathbf{p}) \cdot v + d$, with $\tilde{b}(\mathbf{z}, \mathbf{p}) = \frac{\partial L_{\mathbf{f}}^M h(\mathbf{x})}{\partial v} > 0$. This inequality holds for all possible operating points of the fuel cell system due to physical conditions for the signs of the parameters contained in the vector $\mathbf{p}$. This furthermore guarantees that the state $\vartheta_{1,M,1}$ is the flat system output, allowing also for a design of flatness-based and feedback linearizing controllers.

3.2 Sliding Mode Control for the Flat System Output

To design the interval-based sliding mode controller, the tracking error of all components of $\mathbf{z}$ is defined by the time

derivatives $\tilde{z}_1^{(j)} = z_1^{(j)} - z_{1,d}^{(j)}$ with $j = 0, ..., \delta - 1 = M - 1$ and the system output $\vartheta_{1,M,1} = z_1 = z_1^{(0)}$. Perfect tracking of a given trajectory $z_{1,d}^{(j)}$ corresponds to states which are located on the sliding surface

$$s(\tilde{\mathbf{z}}) = \tilde{z}_1^{(M-1)} + \alpha_{M-2}\tilde{z}_1^{(M-2)} + \ldots + \alpha_0 \tilde{z}_1^{(0)} = 0 \ . \quad (11)$$

To guarantee asymptotic stability of the dynamics on this sliding surface, the parameters $\alpha_0, \ldots, \alpha_{M-2}$ have to be chosen as coefficients of a Hurwitz polynomial of order $M-1$. Moreover, the stabilization of $\mathbf{z}$ towards the sliding surface can be achieved for $s \neq 0$ if a variable structure control law is defined on the basis of the Lyapunov function $V = \frac{1}{2}s^2 > 0 \quad \text{for} \quad s \neq 0$. For the derivation of this control law, the derivative $\dot{V} = s \cdot \dot{s} \leq 0$ is replaced by $s \cdot \dot{s} \leq -\eta \cdot |s| = -\eta \cdot s \cdot \text{sign}\{s\}$, $\eta > 0$ with

$$\begin{aligned} \dot{s}(\tilde{\mathbf{z}}) &= \tilde{z}_1^{(M)} + \alpha_{M-2}\tilde{z}_1^{(M-1)} + \ldots + \alpha_0 \tilde{z}_1^{(1)} \\ &= \tilde{a}(\mathbf{z}, \mathbf{p}, d) + \tilde{b}(\mathbf{z}, \mathbf{p}) \cdot v - z_{1,d}^{(M)} \\ &\quad + \alpha_{M-2}\tilde{z}_1^{(M-1)} + \ldots + \alpha_0 \tilde{z}_1^{(1)}. \end{aligned} \quad (12)$$

Furthermore, $s \cdot \dot{s} \leq -\eta \cdot s \cdot \text{sign}\{s\}$ can be reformulated as $s \cdot (\dot{s} + \eta \cdot \text{sign}\{s\}) \leq 0$ which is guaranteed for

$$\dot{s} + \eta \cdot \text{sign}\{s\} = -\beta \cdot \text{sign}\{s\} \quad (13)$$

with $\eta, \ \beta > 0$. The substitution of $\dot{s}$ defined by (12) for the corresponding term in (13) yields the control law

$$[v] := \left[\frac{-\tilde{a}\,(\mathbf{z}, \mathbf{p}, d) + z_{1,d}^{(M)} - \alpha_{M-2}\tilde{z}_1^{(M-1)} \ldots - \alpha_0 \tilde{z}_1^{(1)}}{\tilde{b}\,(\mathbf{z}, \mathbf{p})} - \frac{1}{\tilde{b}\,(\mathbf{z}, \mathbf{p})} \underbrace{(\eta + \beta)}_{=:\tilde{\eta} > 0} \cdot \text{sign}\{s\} \right] \Bigg|_{\substack{\mathbf{p} \in [\mathbf{p}] \\ d \in [d]}} . \quad (14)$$

During the interval-based evaluation of (14) by means of the toolbox C-XSC (Krämer, n.a.) in a real-time rapid control prototyping environment (a point-valued term d is estimated by the procedures presented in (Dötschel et al., 2013b)), the following cases have to be distinguished for the controller output to guarantee asymptotic stability despite the uncertainties $[\mathbf{p}]$ and $[d]$:

$$v := \begin{cases} \overline{v} := \sup\{[v]\} & \text{for} \quad s \geq 0 \\ \underline{v} := \inf\{[v]\} & \text{for} \quad s < 0 \ . \end{cases} \quad (15)$$

Here, s is evaluated directly for measured data. Simulation results for this control law are presented in (Rauh et al., 2013b) for the scenarios (I) and (II) together with a feedback linearizing controller for the heat-up phase.

For the practical implementation of the controller on a real test rig, it is necessary to determine a pair of variables $\dot{m}_{CG}^{<l^*>}$, $\Delta\vartheta^{<l^*>} := \vartheta_{CG}^{<l^*>} - \vartheta_{1,1,1}$ in each point of time in such a way that (15) is guaranteed to be satisfied. This can be achieved by a real-time minimization of the criterion

$$\begin{aligned} \left[J_\nu^{<l>}\right] = \kappa_1 \cdot \left(\left[\Delta\vartheta_\nu^{<l>}\right]\right)^2 + \kappa_2 \cdot \left(\left[\dot{m}_{CG,\nu}^{<l>}\right]\right)^2 + \\ \kappa_3 \cdot \left(\left[\Delta\vartheta_\nu^{<l>}\right] - \left[\Delta\vartheta_{\nu-1}\right]\right)^2 + \\ \kappa_4 \cdot \left(\left[\dot{m}_{CG,\nu}^{<l>}\right] - \left[\dot{m}_{CG,\nu-1}\right]\right)^2 \ . \end{aligned} \quad (16)$$

The criterion (16) is evaluated at equidistant points of time t_ν and penalizes the variation of the temperature difference $\Delta\vartheta^{<l^*>}$ between two subsequent sampling points $t_{\nu-1}$ and t_ν, the absolute value of $\Delta\vartheta^{<l^*>}$, and the corresponding variation of the mass flow $\dot{m}_{CG}$ as well as its absolute value. The factors κ_1 and κ_2 in (16) have to be chosen such that the control procedure becomes efficient from an energy point of view, while the terms κ_3 and κ_4 aim at the prevention of unnecessarily large variations of the actual control signals. As described in (Rauh et al., 2013b), the corresponding optimization procedure can be implemented by means of an online-applicable interval subdivision procedure. The actual control vector

$$\mathbf{u} := \left[\text{mid}\left[\dot{m}_{CG,\nu}^{<l^*>}\right] \quad \text{mid}\left[\Delta\vartheta_\nu^{<l^*>}\right]\right]^T \in \mathbb{R}^2 \quad (17)$$

is obtained for the subinterval

$$l^* = \arg\,\min_{l=1,\ldots,L}\{\inf\left[J_\nu^{<l>}\right]\} \quad (18)$$

out of L admissible candidates that are characterized by

$$v := \begin{cases} \overline{v} < \inf\{\left[\dot{m}_{CG}^{<l>}\right] \cdot \left[\Delta\vartheta^{<l>}\right]\} & \text{for } s(t) \geq 0 \\ \underline{v} > \sup\{\left[\dot{m}_{CG}^{<l>}\right] \cdot \left[\Delta\vartheta^{<l>}\right]\} & \text{for } s(t) < 0 \ . \end{cases} \quad (19)$$

The control law derived above has been implemented for the SOFC test rig. Fig. 3 shows the cathode gas mass flow $\dot{m}_{CG}$ (solid line) and the cathode gas temperature ϑ_{CG} (solid line) computed by the interval-based sliding mode control structure. According to the procedure described above, these inputs guarantee asymptotic stability. Furthermore, in Figs. 3(a) and 3(b) the temperature trajectory ϑ_{AG} of the anode gas and its constant mass flow $\dot{m}_{AG}$ of nitrogen N_2 are shown for the complete heat-up process of the SOFC stack starting at $\vartheta_{FC} = 297.0$K and ending at a temperature of $\vartheta_{FC} = 473.0$K in a time horizon of $T_{exp} = 23,000$s. Fig. 4(a) shows the desired trajectory $\vartheta_{FC,d}$ and the actual time response of ϑ_{FC}. The resulting error signal $e = \vartheta_{FC,d} - \vartheta_{FC}$, depicted in Fig. 4(b) highlights the excellent tracking behavior that becomes possible from the online evaluation of the interval-based sliding mode (ISM) control law.

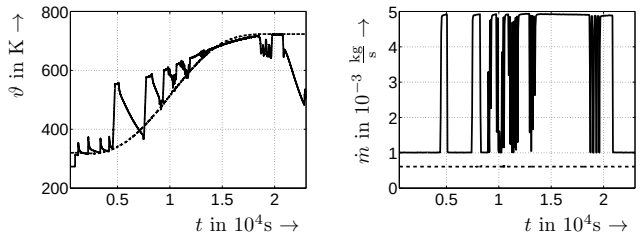

(a) Temperatures ϑ_{AG} (dashed line) and ϑ_{CG} (solid line).

(b) Mass flows $\dot{m}_{AG}$ (dashed line) and $\dot{m}_{CG}$ (solid line).

Fig. 3. Stack inputs during the heat-up phase.

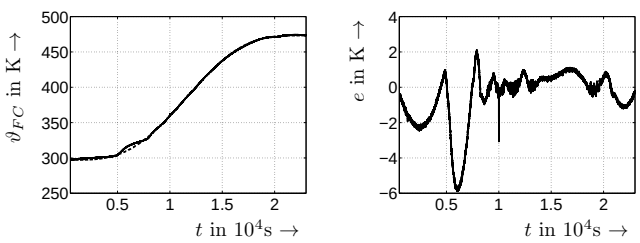

(a) Desired and actual stack module temperatures $\vartheta_{FC,d}$ (dashed) and ϑ_{FC} (solid).

(b) Deviation e between the desired trajectory and the actual stack temperature.

Fig. 4. Experimental validation of the ISM controller.

3.3 Tracking Control for Non-Flat System Outputs

If a non-flat output is chosen as the temperature to be controlled, i.e., $\vartheta_{1,i,1}$ $(i < M)$ in the case (II) or typically any state in the case (III), a transformation is performed as in (9), (10). However, then $\delta < n_x$ holds for the relative degree. Since bounded control inputs lead to bounded states of the model (3), it is possible to use the equation (10) also in this case to design a reliable controller after the following modification: All states that are not parameterizable by (9) and (10) have to be estimated in real time and included in (14) as uncertain parameters. Further details about the interval-based sliding mode controller as well as the influence of actuator constraints are summarized in (Rauh et al., 2013b).

4. SENSITIVITY-BASED PREDICTIVE CONTROL

4.1 Derivation and Experimental Validation

As an *alternative* to the two-stage control procedure described in Sec. 3, a sensitivity-based procedure can be implemented. It is based on the analysis of the sensitivity of the solution $\mathbf{x}(t)$ to the set of ODEs $\dot{\mathbf{x}}(t) = \mathbf{f}(\mathbf{x}(t), \xi)$ with respect to a time-invariant parameter vector $\xi \in \mathbb{R}^{n_\xi}$.

Defining the new state vectors $\mathbf{s}_i(t) := \frac{\partial \mathbf{x}(t)}{\partial \xi_i} \in \mathbb{R}^{n_x}$ for all $i = 1, \ldots, n_\xi$, the sensitivity equations

$$\dot{\mathbf{s}}_i(t) = \frac{\partial \mathbf{f}(\mathbf{x}(t), \xi)}{\partial \mathbf{x}} \cdot \mathbf{s}_i(t) + \frac{\partial \mathbf{f}(\mathbf{x}(t), \xi)}{\partial \xi_i} \tag{20}$$

with the initial conditions $\mathbf{s}_i(0) = \frac{\partial \mathbf{x}(0,\mathbf{p})}{\partial \xi_i}$ can be derived. Note, that $\mathbf{s}_i(0) = \mathbf{0}$ holds if $\mathbf{x}(0)$ is independent of ξ_i.

Now, the control error

$$J = \sum_{\mu=\nu}^{\nu+N_p} \mathcal{D}(\mathbf{y}(t_\mu) - \mathbf{y}_d(t_\mu)) \tag{21}$$

between the actual and desired outputs $\mathbf{y}(t)$ and $\mathbf{y}_d(t)$, respectively, is defined to achieve accurate trajectory tracking. The minimization of J is performed over N_p prediction steps in real time by means of an analytic representation of the output vector $\mathbf{y}(t) = \mathbf{h}(\mathbf{x}(t), \mathbf{u}(t))$ in terms of the states $\mathbf{x}(t)$ and the control signal $\mathbf{u}(t)$ assumed to be piecewise constant for $t_\nu \le t < t_{\nu+1}$.

After computing the differential sensitivity of J by using algorithmic differentiation (Griewank and Walther, 2008), a piecewise constant control $\mathbf{u}(t_\nu)$ can be computed with

$$\mathbf{u}(t_\nu) = \mathbf{u}(t_{\nu-1}) + \Delta\mathbf{u}_\nu \quad \text{and} \quad \Delta\mathbf{u}_\nu = -\left(\frac{\partial J}{\partial \Delta\mathbf{u}_\nu}\right)^+ \cdot J\,, \tag{22}$$

where $\mathbf{M}^+ := \left(\mathbf{M}^T\mathbf{M}\right)^{-1}\mathbf{M}^T$ is the left pseudo-inverse of the matrix $\mathbf{M}$. Here, the sensitivity of J is computed in terms of $\frac{\partial \mathbf{x}(t_\mu)}{\partial \Delta\mathbf{u}_\nu}$ according to (20) by means of a suitable discretization scheme with $\mathbf{u} = \mathbf{u}(t_{\nu-1}) + \Delta\mathbf{u}_\nu$, $\Delta\mathbf{u}_\nu = \mathbf{0}$, where $\frac{\partial \mathbf{x}(t_{\nu-1})}{\partial \Delta\mathbf{u}_\nu} = \mathbf{0}$ holds. For that purpose, the control variations $\Delta\mathbf{u}_\nu$ are interpreted in the same way as the time-invariant parameters ξ in (20).

If interval uncertainties are taken into account for system parameters, control inputs, and measured outputs, the control signal can be computed with

$$\Delta\mathbf{u}_\nu = -\sup\left(\left(\frac{\partial [J]}{\partial \Delta\mathbf{u}_\nu}\right)^+ \cdot [J]\right)\,. \tag{23}$$

After evaluating the control law (22), the state equations are simulated by a suitable interval method for the complete prediction horizon with the updated system input. This simulation leads to guaranteed enclosures of all reachable states over the corresponding horizon (Rauh et al., 2012b). The updated input signal is applied to the system for the time interval $[t_\nu\,;\,t_{\nu+1}]$ if no violation of state constraints is detected over the time interval $\left[t_\nu\,;\,t_{\nu+\tilde{N}_p}\right]$ with $\tilde{N}_p \le N_p$. However, if a possible violation of state constraints is detected (here, by overshooting the maximum admissible state values), a further adjustment of the control input $\mathbf{u}(t_\nu) := \mathbf{u}(t_\nu) + \Delta\tilde{\mathbf{u}}_\nu$ becomes necessary with

$$\Delta\tilde{\mathbf{u}}_\nu = -\sup\left(\left(\frac{\partial [\mathbf{y}]}{\partial \Delta\tilde{\mathbf{u}}_\nu}\right)^+ \cdot \overline{\Delta\mathbf{y}_\nu}\right)\,. \tag{24}$$

Then, the term

$$\overline{\Delta\mathbf{y}_\nu} := \max_{t\in\left[\nu\,;\,t_{\nu+\tilde{N}_p}\right]} \{0\,;\,\sup([\mathbf{y}(t)] - \mathbf{y}_d(t))\}\,, \tag{25}$$

where the *max* and *sup* operators are defined componentwise, denotes the maximum possible overshoot of the desired trajectory over the prediction horizon.

In Fig. 5, the performance criterion

$$\begin{aligned}\mathcal{D} = {} & \kappa_1 \cdot \bar{\vartheta}_{FC}^2 + \kappa_2 \cdot \Delta\vartheta_{FC}^2 + \kappa_3 \cdot (\dot{m}_{CG} - \dot{m}_{CG,d})^2 \\ & + \kappa_4 \cdot (\vartheta_{CG} - \vartheta_{FC,d})^2 + \kappa_5 \cdot \Delta\dot{m}_{CG}^2 + \kappa_6 \cdot \Delta\vartheta_{CG}^2\end{aligned} \tag{26}$$

with a representative mass flow $\dot{m}_{CG,d}$, the spatial variance $\Delta\vartheta_{FC}^2$ of the stack module temperatures $\vartheta_{i,j,k}$ (simplifying to zero in case (I)), and $\Delta\tilde{\mathbf{u}}_\nu = [\Delta\dot{m}_{CG} \quad \Delta\vartheta_{CG}]^T$ has been used to implement a robust tracking controller for the model (I). A suitable choice of the weighting factors leads to control inputs (Fig. 5(b)) which are smoother than in the case of a pure sliding mode control. The resulting control errors in Fig. 5(a) for $t \in [4,000\,;\,13,000]$ s are caused by a reduction of T_{exp} by a factor of two as compared to the previous experiment, where all initial and final temperatures are left unchanged. This causes the preheater to reach its saturation value during this time interval. Moreover, the preheater dynamics (cf. the curves in Fig. 5(b) for a graphical representation) have not been accounted for explicitly in this paper (Rauh et al., 2013a).

This model error is better compensated by the sliding mode controller than by the predictive one. This holds especially for phases where ϑ_{CG} has to be reduced. To further reduce the error $\bar{\vartheta}_{FC} = \vartheta_{FC,d} - \vartheta_{FC}$, it is necessary to prevent saturations of the preheaters. For that purpose, an automatic time-scaling of the desired trajectory $\mathbf{y}_d := \vartheta_{FC,d}$ can be used in future work which makes use of sensitivity-based methods (Rauh et al., 2012b).

4.2 Possible Extensions of the Control Procedure

If the sensitivity-based control procedure is applied to the thermal subsystem of the SOFC, the state equations (3) are evaluated in a discrete-time form over the complete prediction horizon $\left[t_\nu\,;\,t_{\nu+N_p}\right]$, $\mu > \nu$, according to

$$\vartheta_{i,j,k}(t_\mu) \in [\vartheta_{i,j,k}(t_{\mu-1})] + T \cdot \left[\dot{\vartheta}_{i,j,k}(t_{\mu-1})\right] \tag{27}$$

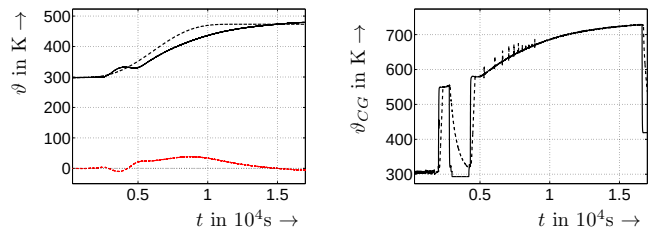

(a) Desired/ actual temperatures $\vartheta_{FC,d}$ (black, dashed)/ ϑ_{FC} (black, solid) and its error.

(b) Computed (solid) and actual (dashed) preheater temperatures ϑ_{CG} for the cathode gas.

Fig. 5. Experimental validation of the predictive controller.

with $\mathbf{u} = \mathbf{u}(t_{\nu-1})$. As it is typical for the naive application of interval methods, this computation of state enclosures might lead to a significant amount of overestimation and, hence, to unnecessarily conservative control laws. Therefore, parts of the state enclosures have to be detected which are certainly caused by overestimation. For that purpose, an energy-related criterion can be derived. It can firstly be evaluated at each point of time t_μ by

$$E_\mu \in [E(t_\mu)] = \sum_{i,j,k} [\vartheta_{i,j,k}(t_\mu)] \tag{28}$$

and, secondly, by

$$E_\mu \in \left[\tilde{E}_\mu\right] := [E_\nu] + \sum_{\zeta=\nu}^{\mu} \left(\sum_{i,j,k} \left[\dot{\vartheta}_{i,j,k}(t_\zeta)\right] \right) \quad , \tag{29}$$

where t_ν is the starting point of the prediction horizon for which the performance criterion J is evaluated. Especially, with respect to the detection of the worst-case overshoot over the desired trajectory for the stack temperature, this criterion can significantly reduce the conservativeness with respect to the maximum predicted temperature for all $t \in \left[t_\nu \,;\, t_{\nu+N_p}\right]$ by the following consistency test: Firstly, the interval vector $[\mathbf{x}(t_\mu)]$ is subdivided into subintervals $[\mathbf{x}'(t_\mu)]$ along its longest edge. Then,

$$E'_\mu \in \left[E'_\mu\right] = \sum_{i,j,k} \left[\vartheta'_{i,j,k}(t_\mu)\right] \tag{30}$$

is evaluated for $[\mathbf{x}'(t_\mu)]$ according to (28).

The subinterval $[\mathbf{x}'(t_\mu)]$ is guaranteed to be caused by overestimation if $\left[E'_\mu\right] \cap \left[\tilde{E}_\mu\right] = \emptyset$ holds. In the case $\left[E'_\mu\right] \subseteq \left[\tilde{E}_\mu\right]$, $\left[\tilde{E}_\mu\right]$ is consistent with (29). All further intervals, for which $\left[E'_\mu\right] \cap \left[\tilde{E}_\mu\right] \neq \emptyset$ and $\left[E'_\mu\right] \not\subseteq \left[\tilde{E}_\mu\right]$ holds, are undecided and can be examined after further subdivision. The evaluation of $[J]$ is then again performed for the reduced predicted overshoot. All further update rules for the piecewise constant predictive control law remain unchanged. The experimental validation of this extension will be one of the upcoming research topics.

5. CONCLUSIONS AND OUTLOOK

In this paper, control strategies have been presented which make use of real-time capable interval arithmetic tools. Besides sliding-mode-type controllers, sensitivity-based model predictive controllers have been used which allow for handling bounded parameter uncertainties and disturbances. A practical verification of these control procedures has been performed on an SOFC test rig at the Chair of Mechatronics, University of Rostock. Future work will deal with improving the spatial resolution of the underlying system models and with an inclusion of real-time capable state and parameter estimators in the experimental validation. Finally, further control procedures will be developed for rapid changes of high-temperature operating points which result from variable electrical loads.

REFERENCES

Bove, R. and Ubertini, S. (eds.) (2008). *Modeling Solid Oxide Fuel Cells*. Springer, Berlin.

Dötschel, T., Auer, E., Rauh, A., and Aschemann, H. (2013a). Thermal Behavior of High-Temperature Fuel Cells: Reliable Parameter Identification and Interval-Based Sliding Mode Control. *Soft Computing*. In print.

Dötschel, T., Rauh, A., Senkel, L., and Aschemann, H. (2013b). Experimental Validation of Interval-Based Sliding Mode Control for Solid Oxide Fuel Cell Systems. In *Proc. of the European Control Conference ECC 2013*. Zurich, Switzerland.

Griewank, A. and Walther, A. (2008). *Evaluating Derivatives: Principles and Techniques of Algorithmic Differentiation*. SIAM, Philadelphia.

Krämer, W. (n.a.). XSC Languages (C-XSC, PASCAL-XSC) — Scientific Computing with Validation, Arithmetic Requirements, Hardware Solution and Language Support. `www.math.uni-wuppertal.de/~xsc/`.

Marquez, H. (2003). *Nonlinear Control Systems*. John Wiley & Sons, Inc., New Jersey.

Rauh, A., Dötschel, T., and Aschemann, H. (2011). Experimental Parameter Identification for a Control-Oriented Model of the Thermal Behavior of High-Temperature Fuel Cells. In *CD-Proc. of IEEE Intl. Conference on Methods and Models in Automation and Robotics MMAR*. Miedzyzdroje, Poland.

Rauh, A., Dötschel, T., Auer, E., and Aschemann, H. (2012a). Interval Methods for Control-Oriented Modeling of the Thermal Behavior of High-Temperature Fuel Cell Stacks. In *Proc. of 16th IFAC Symposium on System Identification SysID 2012*. Brussels, Belgium.

Rauh, A., Kersten, J., Auer, E., and Aschemann, H. (2012b). Sensitivity-Based Feedforward and Feedback Control for Uncertain Systems. *Computing*, (2–4), 357–367.

Rauh, A., Senkel, L., and Aschemann, H. (2012c). Sensitivity-Based State and Parameter Estimation for Fuel Cell Systems. In *Proc. of 7th IFAC Symposium on Robust Control Design*. Aalborg, Denmark.

Rauh, A., Senkel, L., and Aschemann, H. (2013a). Design and Experimental Validation of Control Strategies for Commercial Gas Preheating Systems. In *18th International Conference on Methods and Models in Automation and Robotics*. Miedzyzdroje, Poland. Accepted.

Rauh, A., Senkel, L., Dötschel, T., Auer, E., and Aschemann, H. (2013b). Sliding Mode Control for Uncertain Thermal SOFC Models with Physical Actuator Constraints. In *Proc. of the 15th GAMM-IMACS Intl. Symposium on Scientific Computing, Computer Arithmetic, and Validated Numerics SCAN 2012*. Novosibirsk, Russia. Under review for Reliable Computing.